Geomechanics and Engineering, *Vol. 28, No. 3 (2022) 299-311*
https://doi.org/10.12989/gae.2022.28.3.299

Mechanical model for analyzing the water-resisting key stratum to evaluate water inrush from goaf in roof

Kai Ma[1,2a], Tianhong Yang*[1,2], Yong Zhao[1,2b], Xiangang Hou[1,2c], Yilong Liu[1,2d], Junxu Hou[1,2e], Wenxian Zheng[3f] and Qiang Ye[3g]

[1]*Center for Rock Instability and Seismicity Research, School of Resources and Civil Engineering, Northeastern University, Shenyang 110819, China*
[2]*Key Laboratory of Ministry of Education on Safe Mining of Deep Metal Mines, Northeastern University, Shenyang 110819, China*
[3]*Xiqv Mine, Shanxi Xishan Coal Power Co., Ltd, Taiyuan 030200, China*

(Received May 10, 2021, Revised June 16, 2021, Accepted September 14, 2021)

Abstract. Water-resisting key stratum (WKS) between coal seams is an important barrier that prevents water inrush from goaf in roof under multi-seam mining. The occurrence of water inrush can be evaluated effectively by analyzing the fracture of WKS in multi-seam mining. A "long beam" water inrush mechanical model was established using the multi-seam mining of No. 2+3 and No. 8 coal seams in Xiqu Mine as the research basis. The model comprehensively considers the pressure from goaf, the gravity of overburden rock, the gravity of accumulated water, and the constraint conditions. The stress distribution expression of the WKS was obtained under different mining distances in No. 8 coal seam. The criterion of breakage at any point of the WKS was obtained by introducing linear Mohr strength theory. By using the mechanical model, the fracture of the WKS in Xiqu Mine was examined and its breaking position was calculated. And the risk of water inrush was also evaluated. Moreover, breaking process of the WKS was reproduced with Flac3D numerical software, and was analyzed with on-site microseismic monitoring data. The results showed that when the coal face of No. 8 coal seam in Xiqu Mine advances to about 80 m ~ 100 m, the WKS is stretched and broken at the position of 60 m ~ 70 m away from the open-off cut, increasing the risk of water inrush from goaf in roof. This finding matched the result of microseismic analysis, confirming the reliability of the water inrush mechanical model. This study therefore provides a theoretical basis for the prevention of water inrush from goaf in roof in Xiqu Mine. It also provides a method for evaluating and monitoring water inrush from goaf in roof.

Keywords: goaf; mechanical model; multi-seam mining; water inrush; water-resisting key stratum

1. Introduction

Continuous extraction of underground coal resources have led to the production of numerous goafs (Li *et al*. 2020, Xue *et al*. 2020, Ma *et al*. 2020, Gee *et al*. 2020, Cui *et al*. 2020). These goafs often cause a series of environmental and safety problems such as surface subsidence and spontaneous combustion among other problems (Chen *et al*. 2019, Wang *et al*. 2019, Szurgacz *et al*. 2020, Srivastava *et al*. 2020, Ray *et al*. 2007). Among these problems, water inrush from goafs is a major water hazard that threatens the exploitation of coal resources in China. In the past 10 years, water inrush accidents from goafs have accounted for more than 70% of all water hazard accidents. In the same line, water inrush accidents from goafs have increased to more than 90% over the past five years (Wu. 2014). The downward mining method is used to mine multiple coal seams in many mining areas. After the upper coal has been mined, the goaf is closed so that water continues to accumulate in the goaf to form a water-logged goaf. When mining the lower coal, water inrush from the goaf in roof may occur thus leading to suspension of mining. It can also lead to injuries to the mine workers. Cognizant to this, it is therefore necessary to identify and analyze the problems associated with water inrush from goaf in roof during multi-seam mining.

Water inrush from goaf in roof is a combination of water inrush from goaf and water inrush from roof. Currently, scholars have majorly focused on water inrush from the goaf or the roof. However, less focus has been put in studying water inrush from goaf in roof, especially its mechanism of water inrush. Although some scholars have postulated the concept of "water-resisting control strata" to study the problem of water inrush from goaf in roof based on damage mechanics (Feng *et al*. 2019), they failed to the analysis of damage process. In addition, most of the research done on water inrush from goaf has mainly focused on goaf in single coal seam. Huang *et al*. (2018)

*Corresponding author, Ph.D.
E-mail: yang_tianhong@126.com
[a]Ph.D. Student
E-mail: 1208988922@qq.com
[b]Ph.D.
[c]Ph.D.
[d]Ph.D.
[e]Ph.D.
[f]Ph.D.
[g]Ph.D.

ISSN: 2005-307X (Print), 2092-6219 (Online)

studied the lateral boundary value of water-permeable fractured zone under single coal mining. Dou *et al*. (2012) found that there was an internal relationship between micro-seismic events and water inrush while using a micro-seismic monitoring method to predict water inrush from goaf under single coal mining. Besides, in the studies of water inrush from roof, majority of the water sources were geological aquifers and not water-logged goafs (Chen *et al*. 2020, Wu *et al*. 2016, Rashid *et al*. 2020, Kromkova *et al*. 2020, Zhang *et al*. 2020). Whether the development height of the water-permeable fractured zone can reach the elevation of the aquifer is key for evaluating water inrush from the roof. Field measurement of the height of the water-permeable fractured zone in China's major mining areas led to development of an empirical formula that has a good adaptability and practicability. The formula is used in estimation of the height of the water-permeable fractured zone in the field (Qu *et al*. 2015, Coal Industry Bureau of China. 2000). However, proposal of the "key stratum" analysis method have led to advancements in determination of the height of the water-permeable fractured zone (Qian. 2010). The height of the water-permeable fractured zone has been found to be related to the position, strength and thickness of the key stratum (Xu *et al*. 2012, Wang *et al*. 2019). Under single coal mining, the stability of the water-resisting key stratum (WKS) plays a critical role in evaluation of water inrush from the roof. In specific stope conditions, some scholars simplified the key stratum in the roof to an elastic thin plate with four fixed edges, one pair of simple-supported edges and another pair of fixed edges, three fixed edges and the other simple-supported edge, or two fixed adjacent sides and the other simple-supported adjacent sides to study the fracture of the key stratum under the uniform load of overburden rock by elastic mechanics (Liu *et al*. 2018, Wang *et al*. 2011, Jiang *et al*. 2014, Jiang *et al*. 2015). Although a more accurate solution can be obtained using this method, it is difficult to use the method in cases of non-uniform load. For this reason, the key stratum was simplified to be either a fixed beam or cantilever beam to analyze the bending and breaking of the key stratum with material mechanics (Wang *et al*. 2019, Li *et al*. 2018). Reliable results were obtained using the simplified key stratum thus providing a reference for analyzing the stability of the WKS between coal seams in evaluating the occurrence of water inrush from goaf in roof.

Under multi-seam mining, the loading state of the WKS between coal seams is more complex. In the water inrush mechanical model, pressure from the goaf, the gravity of overburden rock, the gravity of accumulated water, and the constraint conditions should be considered based on the actual situation. Herein, the WKS was simplified to a long beam with one fixed end and the other simple-supported end to calculate the stress distribution of the beam during the mining process of No. 8 coal seam. This was based on a case of multi-seam mining of No. 2+3 and No. 8 coal seams in Xiqu Mine, Shanxi Province, China. Then, the linear Mohr strength theory was employed to obtain the mechanical criterion of breakage at any point of the WKS. Next, the water inrush mechanical model was used to evaluate the fracture of the WKS in Xiqu Mine and calculate its breaking position, which could effectively evaluate water inrush risk. Finally, the breaking process of WKS was reproduced using the Flac3D numerical software and analyzed with on-site micro-seismic monitoring data to obtain reliable conclusions that could provide solutions for the prevention of water inrush from goaf in roof in Xiqu Mine.

2. Engineering background

Xiqu Mine is in Gujiao City, Shanxi Province, China. The stable coal seams in the mining area are mainly No. 2+3 and No. 8. The thickness of No. 2+3 coal seam is 5 m and its mining depth is 187 m. The thickness of No. 8 coal seam is 4 m and its mining depth is 249 m. The distance between two coal seams is 58 m. Two coal seams are successively mined by the downward mining method. The caving method is used for roof management. When mining two coal seams, open-off cuts are roughly in the same vertical plane. The length of the coal face is 130 m in No. 2+3 coal seam and 220 m in No. 8 coal seam (Fig. 1). With the advancements of coal faces, the whole thickness of the coal is mined at one time along the strike. Currently, No. 8 coal seam is being mined. No. 2+3 coal seam has been exhausted. Over time, many small coal mines have exploited the No. 2+3 coal seam leading to formation of many water accumulation areas. In addition, after mining in No. 2+3 coal seam, a water-permeable fractured zone developed in the roof. The fractured zone allowed bedrock fissure water, loose bed water and surface water to continually accumulate in the goaf through the water-conducting fissures thus resulting in formation of a water-logged goaf. In fact, before, the detection results have shown that there was a large area of accumulated water in the goaf in the No. 2+3 coal seam even before mining started in the No. 8 coal seam.

Accumulated water in No. 2+3 coal seam must pass through the stratums (58 m) between the two coal seams to reach the coal face of No. 8 coal seam to form a water inrush (Fig. 1). The geological histogram of the stratums between the two coal seams is shown in Fig. 2. Based on the most relevant recent study, the key stratum is often thick and not easy to break (Li *et al*. 2018). Cognizant to this, the siltstone stratum with a thickness of 21 m can be the WKS (Fig. 2).

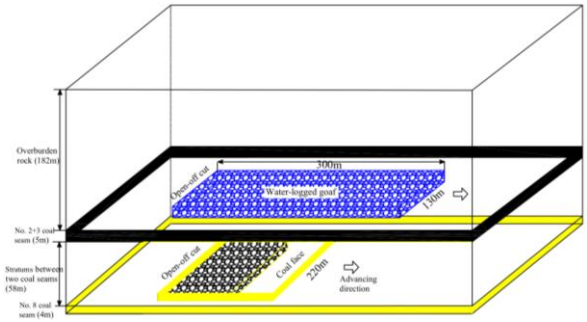

Fig. 1 Spatial location distribution of No. 2+3 and No. 8 coal seams in Xiqu Mine

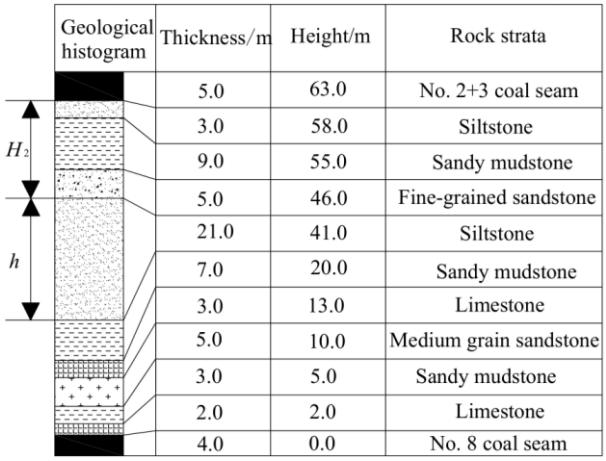

Fig. 2 The geological histogram of the stratums between two coal seams

3. Water inrush mechanical model for the WKS

3.1 Force analysis and model simplification

After mining in No. 2+3 coal seam in Xiqu Mine, the pressure on the stratums below the remaining protective coal pillar increased because of the supporting pressure on the coal pillar. The zone between the coal wall and the goaf is called the pressure recovery zone (PRZ). In this zone, the rock falling into the goaf is gradually compacted causing the pressure on the floor to continue increasing and recovering. The length of the PRZ is x_0 (Fig. 3). In Fig. 3, the zone is referred to as the pressure stability zone (PSZ). In this zone, the pressure on the floor eventually recovers to a certain stable value and does not increase anymore. In practice, the stable pressure is usually less than the original pressure. When the mining depth of No. 2+3 coal seam is H_1 and the average bulk density of the stratums is γ, the original pressure is expressed as γH_1. When a coefficient $0 < k_1 < 1$ is set, the stable pressure is then be expressed as $k_1\gamma H_1$. During mining, the floor repeatedly undergo the compression and expansion because of the mine pressure until a fractured zone known as the floor-failure zone (FFZ) forms(Yin *et al*. 2019, Chen *et al*. 2020). The depth of the FFZ is h_p. The WKS must maintain continuity and not be damaged to maintain a high water-resisting capacity. If the vertical distance from the top surface of the WKS to No. 2+3 coal seam is H_2, then $H_2 \geq h_p$ is required. In shallow mining, h_p is obtained from empirical formula (1) (Li. 1999).

$$h_p = 0.7007 + 0.1079L \tag{1}$$

where L is the length of coal face in No. 2+3 coal seam.

If L is substituted with 130 m in equation (1), h_p is about 14.7 m. In Fig. 2, $H_2 = 17$ m $> h_p$. As such, the WKS is not damaged after the mining of No. 2+3 coal seam. It remains continuous.

Open-off cuts of the two coal seams are roughly in the same vertical plane (Fig. 3). When mining No. 8 coal seam, supporting pressures are formed on both the protective coal pillar and coal body near the coal face. As the coal face

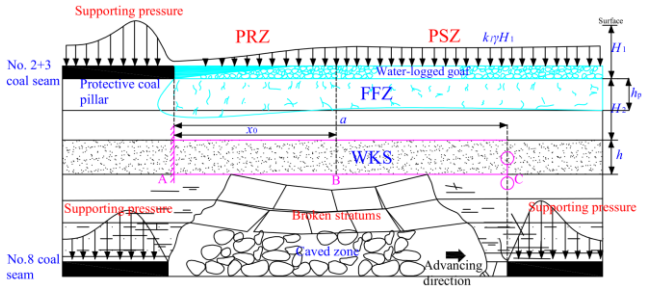

Fig. 3 Force analysis for the WKS in multi-seam mining

advances, the roof stratums close to the coal seam collapse to form a caved zone. The roof stratums farther from the coal seam break and are hinged to each other. The WKS is not easy to break compared with the stratums below it. As such, it is often in a suspended state before breaking. If the advancing distance is a when the WKS breaks, and the influence of the breaking angle of the stratums is ignored, then the length of the suspended section (AC) is approximately equal to a.

The suspended section (AC) of the WKS is simplified to a long beam with a rectangular cross-section. The length of the long beam is a, its height is the thickness h of the WKS and its width is taken as the unit width. At the A-end, the WKS is constrained by the protective coal pillars. It is also under high pressure generated by the supporting pressure. It can thus be regarded as a fixed-end. At the C-end, the WKS is overlapped on the complete stratums below it. The rock mass above it is basically broken and thus cannot effectively restrict the long beam from rotating around the C-end. The constraint at the C-end can be simplified to a movable hinge bearing if the horizontal *in-situ* stress is ignored in shallow mining (Fig. 3). The beam is subjected to the goaf pressure which is simplified as a linearly distributed load in the AB section and a uniformly distributed load with a concentration degree of $k_1\gamma H_1$ in the BC section. In addition, the beam is also affected by the gravity of the stratums above it with a concentration degree of γH_2 and its own gravity with a concentration degree of γh. At the mining site, accumulated water mainly fills the gaps in the goaf. Only a small amount of the water penetrates into the FFZ. Assuming that the crushing expansion coefficient of the rock is k_2 and the height of the accumulated water in the goaf is h_w, q_w (the gravity concentration degree of the accumulated water on the WKS) can be derived from Eq. (2).

$$q_w = \frac{nsh_w\gamma_w}{s} \cdot 1 = \left(\frac{k_2 v - v}{k_2 v}\right) h_w\gamma_w = \left(\frac{k_2 - 1}{k_2}\right) h_w\gamma_w \tag{2}$$

where n denotes the porosity of the collapsed rock mass in goaf, s denotes the projected area of the collapsed rock mass on the WKS, γ_w is the bulk density of accumulated water and v is the volume of the rock mass before collapse.

In Eq. (2), q_w increases with the increase of h_w to reflect the continuous accumulation of water in goaf. The simplified water inrush mechanical model is shown in Fig. 4.

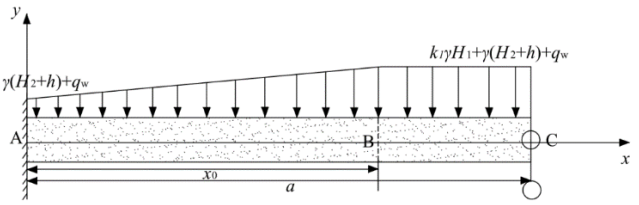

Fig. 4 The "long beam" water inrush mechanical model for the WKS

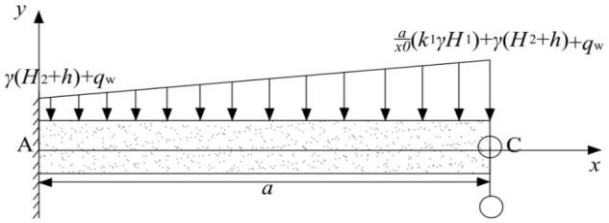

Fig. 5 The water inrush mechanical model for $a \le x_0$

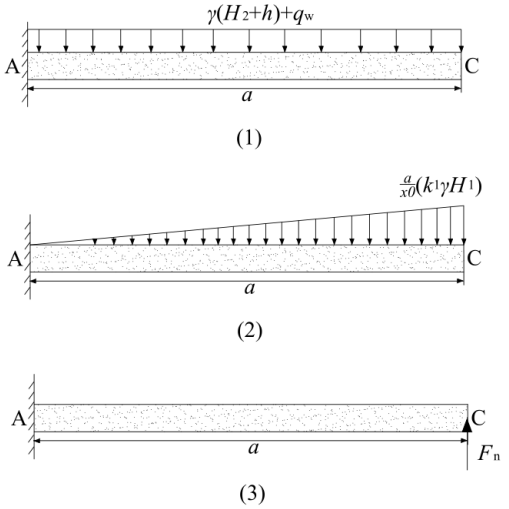

Fig. 6 The superposition mechanical model for $a \le x_0$

3.2 Analysis of the mechanical model

The water inrush mechanical model in Fig. 4 is the bending problem of a statically indeterminate beam. When $a \le x_0$, the beam is only subjected to the linearly distributed load in the AB section. When $a > x_0$, the beam is additionally subjected to a uniformly distributed load in the BC section. In both cases, the bending deformation of the beam is different and is therefore calculated separately. When $a \le x_0$, the water inrush mechanical model is shown in Fig. 5.

First, the constraint reactions at both A and C ends are solved. If the constraint at the C-end is released and replaced by the force F_n, the bending deformation of the beam in the water inrush mechanical model (Fig. 5) is solved by superposition of the three models in Fig. 6. This is done based on the superposition principle.

In Fig. 6, if $q_0 = \gamma(H_2 + h) + q_w$, $q_1 = a/x_0(k_1\gamma H_1)$, the elastic modulus of the beam is E and the moment of inertia of the cross section on the neutral axis is I, then, W_{c1}, W_{c2} and W_{c3} (the deflections at point C) are expressed as follows according to material mechanics

$$W_{c1} = -\frac{q_0 a^4}{8EI} \tag{3}$$

$$W_{c2} = \frac{q_1 a^4}{30EI} - \frac{q_1 a^4}{8EI} \tag{4}$$

$$W_{c3} = \frac{F_n a^3}{3EI} \tag{5}$$

According to the deformation compatibility condition, W_c (the deflection at point C) is equal to 0. That is, $W_{c1} + W_{c2} + W_{c3} = 0$. From this, F_n can be obtained as

$$F_n = \frac{a}{40}\left(15q_0 + 11q_1\right) \tag{6}$$

Based on the equilibrium equations: $\sum F_{(y)} = 0$ and $\sum M_{(A)} = 0$ in the coordinate system in Fig. 5, the constraint reactions at the A-end can be obtained as follows

$$F_A = \frac{a}{40}\left(25q_0 + 9q_1\right) \tag{7}$$

$$M_A = \frac{a^2}{120}\left(15q_0 + 7q_1\right) \tag{8}$$

Once the constraint reactions are obtained, the expressions of the shear equation F_s and the bending moment equation M on the beam can be obtained as

$$F_s = -\frac{q_1}{2a}x^2 - q_0 x + \frac{a}{40}\left(25q_0 + 9q_1\right) \qquad 0 < x < a \tag{9}$$

$$M = -\frac{q_1}{6a}x^3 - \frac{q_0}{2}x^2 + \frac{a}{40}\left(25q_0 + 9q_1\right)x - \frac{a^2}{120}\left(15q_0 + 7q_1\right) \qquad 0 < x \le a \tag{10}$$

The beam is in a state of two-dimensional stress ignoring the effect of horizontal *in-situ* stress. Based on the distributions of shear stress τ_{xy} and normal stress σ_x on the beam at any point of the cross-section, the stress expressions at any position of the entire beam are

$$\sigma_x = \frac{My}{I} = \frac{y}{I}\left[-\frac{q_1}{6a}x^3 - \frac{q_0}{2}x^2 + \frac{a}{40}\left(25q_0 + 9q_1\right)x - \frac{a^2}{120}\left(15q_0 + 7q_1\right)\right] \tag{11}$$

$$\tau_{xy} = \frac{F_s}{2I}\left(\frac{h^2}{4} - y^2\right) = \frac{1}{2I}\left(\frac{h^2}{4} - y^2\right)\left[-\frac{q_1}{2a}x^2 - q_0 x + \frac{a}{40}\left(25q_0 + 9q_1\right)\right] \tag{12}$$

In the two-dimensional stress state, one principal stress is 0 while the other two principal stresses are calculated by the following formula

$$\left.\begin{matrix}\sigma_{max}\\ \sigma_{min}\end{matrix}\right\} = \frac{\sigma_x + \sigma_y}{2} \pm \sqrt{\left(\frac{\sigma_x - \sigma_y}{2}\right)^2 + \tau_{xy}^2} \tag{13}$$

For the bending beam under transverse force, if the longitudinal fibers are not squeezed, σ_y in Eq. (13) is approximately 0. Substituting Eqs. (11) and (12) into Eq. (13) the following formula is obtained

$$\left.\begin{matrix}\sigma_{\max}\\ \sigma_{\min}\end{matrix}\right\} = \frac{y}{2I}\left[-\frac{q_1}{6a}x^3 - \frac{q_0}{2}x^2 + \frac{a}{40}\left(25q_0 + 9q_1\right)x - \frac{a^2}{120}\left(15q_0 + 7q_1\right)\right] \pm \frac{1}{2I}\sqrt{\begin{matrix}y^2\left[-\frac{q_1}{6a}x^3 - \frac{q_0}{2}x^2 + \frac{a}{40}\left(25q_0 + 9q_1\right)x - \frac{a^2}{120}\left(15q_0 + 7q_1\right)\right]^2\\ +\left(\frac{h^2}{4} - y^2\right)^2\left[-\frac{q_1}{2a}x^2 - q_0x + \frac{a}{40}\left(25q_0 + 9q_1\right)\right]^2\end{matrix}} \tag{14}$$

At this point, two principal stresses at any point of the beam are obtained using formula (14). The other principal stress is 0. As such, three principal stresses are obtained. The yielding and failure of the beam is determined by arranging the algebraic values of the three principal stresses from large to small: $\sigma_1 \geq \sigma_2 \geq \sigma_3$, and introducing the linear Mohr strength theory.

$$\sigma_1 - \frac{\sigma_t}{\sigma_c}\sigma_3 \geq \sigma_t \tag{15}$$

where σ_t denotes the uniaxial tensile strength of the WKS and σ_c denotes the uniaxial compressive strength of the WKS.

When $a > x_0$, the resultant water inrush mechanical model is shown in Fig. 4. In the same way, if the constraint at the C-end is released and replaced by the force F_{n1}, the bending deformation of the beam is solved by superposition of the three models in Fig. 7.

In Fig. 7, if $q_2 = k_1\gamma H_1 + \gamma(H_2 + h) + q_w$ and $q_3 = k_1\gamma H_1$, then, W_{c11}, W_{c22} and W_{c33} are expressed as follows

$$W_{c11} = -\frac{q_2 a^4}{8EI} \tag{16}$$

$$W_{c22} = W_{B22} + \left(a - x_0\right)\theta_{B22} = \frac{q_3 x_0^4}{30EI} + \left(a - x_0\right)\frac{q_3 x_0^3}{24EI} \tag{17}$$

$$W_{c33} = \frac{F_{n1}a^3}{3EI} \tag{18}$$

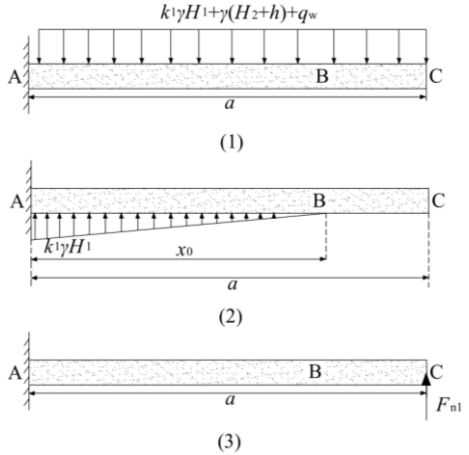

Fig. 7 The superposition mechanical model for $a > x_0$

In equation (17), W_{B22} denotes the deflection at point B in model (2) in Fig. 7 and θ_{B22} denotes the rotation angle at point B in model (2) in Fig. 7.

Similarly, $W_{c11} + W_{c22} + W_{c33} = 0$ based on the deformation compatibility condition. Based on the equilibrium equations: $\sum F_{(y)} = 0$ and $\sum M_{(A)} = 0$, the constraint reactions at the ends of A and C can be obtained as follows

$$F_{n1} = \frac{3}{8}q_2 a - \frac{q_3 x_0^3}{8a^2} + \frac{q_3 x_0^4}{40a^3} \tag{19}$$

$$F_{A1} = \frac{5}{8}q_2 a + \frac{q_3 x_0^3}{8a^2} - \frac{q_3 x_0^4}{40a^3} - \frac{q_3 x_0}{2} \tag{20}$$

$$M_{A1} = \frac{1}{8}q_2 a^2 - \frac{q_3 x_0^4}{40a^2} + \frac{q_3 x_0^3}{8a} - \frac{q_3 x_0^2}{6} \tag{21}$$

The expressions of the shear equation F_{s1} and the bending moment equation M_1 on the beam are obtained as

$$F_{s1} = -\frac{q_1}{2a}x^2 - q_0 x + \frac{5}{8}q_2 a + \frac{q_3 x_0^3}{8a^2} - \frac{q_3 x_0^4}{40a^3} - \frac{q_3 x_0}{2} \qquad 0 < x \leq x_0 \tag{22}$$

$$F_{s1} = -q_2 x + \frac{5}{8}q_2 a + \frac{q_3 x_0^3}{8a^2} - \frac{q_3 x_0^4}{40a^3} \qquad x_0 \leq x < a \tag{23}$$

$$M_1 = -\frac{q_1}{6a}x^3 - \frac{q_0}{2}x^2 + \left(\frac{5}{8}q_2 a + \frac{q_3 x_0^3}{8a^2} - \frac{q_3 x_0^4}{40a^3} - \frac{q_3 x_0}{2}\right)x - \frac{1}{8}q_2 a^2 + \frac{q_3 x_0^4}{40a^2} - \frac{q_3 x_0^3}{8a} + \frac{q_3 x_0^2}{6} \qquad 0 < x \leq x_0 \tag{24}$$

$$M_1 = -\frac{q_2}{2}x^2 + \left(\frac{5}{8}q_2 a + \frac{q_3 x_0^3}{8a^2} - \frac{q_3 x_0^4}{40a^3}\right)x - \frac{1}{8}q_2 a^2 - \frac{q_3 x_0^3}{8a} + \frac{q_3 x_0^4}{40a^2} \qquad x_0 \leq x \leq a \tag{25}$$

Similarly, the stress expressions at any position of the entire beam are

$$\sigma_{x1} = \frac{y}{I}\left[\begin{matrix}-\frac{q_1}{6a}x^3 - \frac{q_0}{2}x^2 + \left(\frac{5}{8}q_2 a + \frac{q_3 x_0^3}{8a^2} - \frac{q_3 x_0^4}{40a^3} - \frac{q_3 x_0}{2}\right)x - \frac{1}{8}q_2 a^2\\ + \frac{q_3 x_0^4}{40a^2} - \frac{q_3 x_0^3}{8a} + \frac{q_3 x_0^2}{6}\end{matrix}\right] \qquad 0 < x \leq x_0 \tag{26}$$

$$\sigma_{x1} = \frac{y}{I}\left[\begin{matrix}-\frac{q_2}{2}x^2 + \left(\frac{5}{8}q_2 a + \frac{q_3 x_0^3}{8a^2} - \frac{q_3 x_0^4}{40a^3}\right)x\\ - \frac{1}{8}q_2 a^2 - \frac{q_3 x_0^3}{8a} + \frac{q_3 x_0^4}{40a^2}\end{matrix}\right] \qquad x_0 \leq x \leq a \tag{27}$$

$$\tau_{xy1} = \frac{1}{2I}\left(\frac{h^2}{4} - y^2\right)\left[\begin{matrix}-\frac{q_1}{2a}x^2 - q_0 x + \frac{5}{8}q_2 a\\ + \frac{q_3 x_0^3}{8a^2} - \frac{q_3 x_0^4}{40a^3} - \frac{q_3 x_0}{2}\end{matrix}\right] \qquad 0 < x \leq x_0 \tag{28}$$

$$\tau_{xy1} = \frac{1}{2I}\left(\frac{h^2}{4} - y^2\right)\begin{bmatrix} -q_2 x + \frac{5}{8} q_2 a + \frac{q_3 x_0^3}{8a^2} \\ -\frac{q_3 x_0^4}{40a^3} \end{bmatrix} \quad x_0 \le x < a \tag{29}$$

By substituting Eqs. (26) and (28) into Eq. (13), and taking $\sigma_y = 0$, the expression of the two principal stresses at any point of the AB section are obtained as follows

$$\begin{Bmatrix} \sigma_{max1} \\ \sigma_{min1} \end{Bmatrix} = \frac{y}{2I}\begin{bmatrix} -\frac{q_1}{6a}x^3 - \frac{q_0}{2}x^2 + \left(\frac{5}{8}q_2 a + \frac{q_3 x_0^3}{8a^2} - \frac{q_3 x_0^4}{40a^3} - \frac{q_3 x_0}{2}\right)x \\ -\frac{1}{8}q_2 a^2 + \frac{q_3 x_0^4}{40a^2} - \frac{q_3 x_0^3}{8a} + \frac{q_3 x_0^2}{6} \end{bmatrix} \pm \frac{1}{2I}\sqrt{\begin{bmatrix} y^2 \begin{bmatrix} -\frac{q_1}{6a}x^3 - \frac{q_0}{2}x^2 + \left(\frac{5}{8}q_2 a + \frac{q_3 x_0^3}{8a^2} - \frac{q_3 x_0^4}{40a^3} - \frac{q_3 x_0}{2}\right)x \\ -\frac{1}{8}q_2 a^2 + \frac{q_3 x_0^4}{40a^2} - \frac{q_3 x_0^3}{8a} + \frac{q_3 x_0^2}{6} \end{bmatrix}^2 \\ + \left(\frac{h^2}{4} - y^2\right)^2 \left[-\frac{q_1}{2a}x^2 - q_0 x + \frac{5}{8}q_2 a + \frac{q_3 x_0^3}{8a^2} - \frac{q_3 x_0^4}{40a^3} - \frac{q_3 x_0}{2}\right]^2 \end{bmatrix}} \tag{30}$$

Similarly, by substituting Eqs. (27) and (29) into Eq. (13), and taking $\sigma_y = 0$, the expression of the two principal stresses at any point of the BC section are obtained as follows

$$\begin{Bmatrix} \sigma_{max1} \\ \sigma_{min1} \end{Bmatrix} = \frac{y}{2I}\begin{bmatrix} -\frac{q_2}{2}x^2 + \left(\frac{5}{8}q_2 a + \frac{q_3 x_0^3}{8a^2} - \frac{q_3 x_0^4}{40a^3}\right)x \\ -\frac{1}{8}q_2 a^2 - \frac{q_3 x_0^3}{8a} + \frac{q_3 x_0^4}{40a^2} \end{bmatrix} \pm \frac{1}{2I}\sqrt{\begin{bmatrix} y^2 \left[-\frac{q_2}{2}x^2 + \left(\frac{5}{8}q_2 a + \frac{q_3 x_0^3}{8a^2} - \frac{q_3 x_0^4}{40a^3}\right)x - \frac{1}{8}q_2 a^2 - \frac{q_3 x_0^3}{8a} + \frac{q_3 x_0^4}{40a^2}\right]^2 \\ + \left(\frac{h^2}{4} - y^2\right)^2 \left[-q_2 x + \frac{5}{8}q_2 a + \frac{q_3 x_0^3}{8a^2} - \frac{q_3 x_0^4}{40a^3}\right]^2 \end{bmatrix}} \tag{31}$$

The other principal stress is 0. The yielded state of the beam is determined using Eq. (15) by arranging the algebraic values of the three principal stresses from large to small: $\sigma_1 \ge \sigma_2 \ge \sigma_3$. Based on the yielded state of WKS, its fracture and the water inrush risk can be evaluated.

3.3 Calculation and evaluation for a case

In order to evaluate water inrush from the multi-seam mining of No. 2+3 and No. 8 coal seams in Xiqu Mine, the fracture and breaking position of the WKS are analyzed using the mechanical model. In Figs. 1 and 2, H_1 = 187 m, H_2 = 17 m, and h = 21 m. Before exploitation of No. 8 coal seam, the accumulated water in the goaf is fully explored and released to prevent the water inrush from goaf in roof. As such, q_w = 0 kN/m. Generally, if x_0 is 60 m, γ is 23 kN/m^3 and k_1 is 0.7, then q_0 = 874 kN/m, $q_1 \approx (50a)$ kN/m, q_2 = 3884.7 kN/m and q_3 = 3010.7 kN/m (Song *et al.* 2019). When $a \le x_0$, the shear equation and the bending moment equation of the beam are obtained from Eqs. (9) and (10).

$$F_s \approx -25x^2 - 874x + 11.3a^2 + 546.3a \tag{32}$$

$$M \approx -8.3x^3 - 437x^2 + \left(11.3a^2 + 546.3a\right)x - 2.9a^3 - 109.3a^2 \tag{33}$$

The shear diagram and bending moment diagram of the beam are shown in Fig. 8.

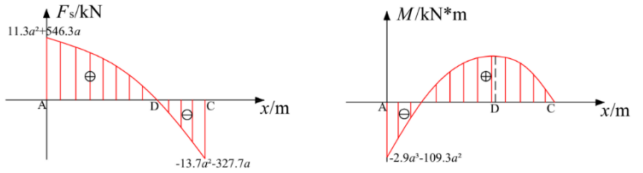

Fig. 8 The shear diagram and bending moment diagram of the beam for $a \le x_0$

When $a > x_0$, the shear equation and the bending moment equation of the beam are obtained from Eqs. (22)-(25).

AB section

$$F_{s1} \approx -25x^2 - 874x + 2427.9a + \frac{81288900}{a^2} - \frac{975466800}{a^3} - 90321 \tag{34}$$

BC section

$$F_{s1} \approx -3884.7x + 2427.9a + \frac{81288900}{a^2} - \frac{975466800}{a^3} \tag{35}$$

AB section

$$M_1 \approx -8.3x^3 - 437x^2 + \left(2427.9a + \frac{81288900}{a^2} - \frac{975466800}{a^3} - 90321\right)x - 485.6a^2 - \frac{81288900}{a} + \frac{975466800}{a^2} + 1806420 \tag{36}$$

BC section

$$M_1 \approx -1942.4x^2 + \left(2427.9a + \frac{81288900}{a^2} - \frac{975466800}{a^3}\right)x - 485.6a^2 - \frac{81288900}{a} + \frac{975466800}{a^2} \tag{37}$$

The shear diagram and bending moment diagram of the beam are shown in Fig. 9.

Continuous advancement of the coal face in No. 8 coal seam causes an increase in the bending moment and shear force of the WKS at position A of the open-off cut which is prone to tensile shear failure. The shear force at position C of the coal face continues to increase easily leading to shear failure. In addition, the shear force of the WKS is 0 at position D. However, the bending moment is at its highest and is thus prone to tensile failure. The WKS is in a unidirectional stress state at position D, and in a bidirectional stress state at positions A and C. In the unidirectional stress state, only normal stress σ_x (principal stress) exists on the cross-section of D. When y = -0.5h on the cross-section of D, the maximum principal tensile stress σ_{xmax} is obtained. Its magnitude is

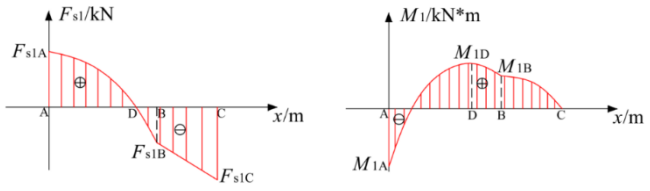

Fig. 9 The shear diagram and bending moment diagram of the beam for $a > x_0$

Table 1 The trial results under different mining distance

a/m	$a \le x_0$	F_{s1B}/kN	$F_{sD} = 0$	x_D/m	M_D/kN*m	$\lvert\sigma_{xmax}\rvert$/MPa	$\lvert\sigma_{xmax}\rvert \ge \sigma_t$	y_p/m
40	Yes		Eq. (32)	26.1	236491	3.2	No	0
50	Yes		Eq. (32)	32.8	423753	5.8	No	0
60	Yes		Eq. (32)	39.5	688351	9.4	Yes	3.8
70	No	-49383	Eq. (34)	46.1	1027606	14.0	Yes	6.0
80	No	-28054	Eq. (34)	52.5	1451490	19.7	Yes	7.3
90	No	-5873	Eq. (34)	58.6	1941028	26.4	Yes	8.1
100	No	16861	Eq. (35)	64.3	2469189	33.6	Yes	8.6

$$\left|\sigma_{xmax}\right| = \frac{M_D h}{2I} \tag{38}$$

Therefore, the discriminant of whether the WKS yields at the cross-section D is

$$\left|\sigma_{xmax}\right| \ge \sigma_t \tag{39}$$

Based on formulas (11) and (39), the yield height y_p of the WKS on the cross-section of D is calculated as follows

$$y_p = \frac{h}{2} - \left|\frac{I\sigma_t}{M_D}\right| \tag{40}$$

If the uniaxial tensile strength σ_t of the WKS is 6 MPa (Li 2011), the trial method is used to calculate the yield position x_D of the WKS under different mining distance a. The stress and yield height of the WKS at position D are thus calculated. When $a \le x_0$, x_D is obtained by setting shear Eq. (32) to 0 and then substituting x_D into the bending moment Eq. (33) to obtain M_D. When $a > x_0$, the shear force F_{s1B} at position B is calculated first from the shear Eq. (35).

The corresponding shear equation and bending moment equation are selected to calculate x_D and M_D by determining whether $F_{s1B} < 0$. If $F_{s1B} < 0$, x_D is obtained by setting shear Eq. (34) to 0, and then substituting x_D into the bending moment Eq. (36) to calculate M_D. Moreover, x_D is obtained by setting shear Eq. (35) to 0, and then substituting x_D into the moment Eq. (37) to obtain M_D. The trial results are shown in Table 1.

Based on Table 1, when the coal face advances about 60 m in No. 8 coal seam, the WKS begins to yield at position D about 40 m from the open-off cut. The yield height is about 3.8 m. The yield position D moves forward continuously as the coal face advances while the yield span and height continue to increase. At an advancing distance of about 100 m, the yield height is up to 8.6 m at a position about 64 m away from the open-off cut. This height is close to the neutral axis of the WKS and is thus prone to tensile breakage.

To calculate the broken positions, it is assumed that the suspended height of the WKS is sufficient. However, in actual mining, the remaining suspended height is limited under the action of crushing expansion of the collapsed stratums below the WKS. Cognizant to this, the displacement condition for the yielding and failure of the WKS thus meet the following requirement: the maximum deflection W_{max} of the WKS is less than the suspended height H_3 when breaking. Generally, the crushing expansion coefficient k_2 is between 1.1 and 1.15. If k_2 is the maximum value (1.15), H_3 = (24-20×1.15) m = 1 m based on Fig. 2. Substituting a = 100 m into the bending moment Eqs. (36) and (37) gives:

AB section

$$M_1 \approx -8.3x^3 - 437x^2 + 159622x - 3764922 \tag{41}$$

BC section

$$M_1 \approx -1942.4x^2 + 249943x - 5571342 \tag{42}$$

According to material mechanics, the relationship between the rotation angle, deflection and bending moment of the beam is as follows

$$\theta = \frac{\mathrm{d}_W}{\mathrm{d}_x} = \int \frac{M}{EI}\,\mathrm{d}_x + \mathrm{C} \tag{43}$$

$$W = \iint \left(\frac{M}{EI}\,\mathrm{d}_x\right)\mathrm{d}_x + \mathrm{C}x + \mathrm{D} \tag{44}$$

Substituting Eqs. (41) and (42) into Eqs. (43) and (44) respectively as well as based on the constraint conditions at ends A and C and the deformation compatibility conditions at B: $W_{(x=0)} = 0$, $\theta_{(x=0)} = 0$, $W_{(x=100)} = 0$, $W_{AB(x=60)} = W_{BC(x=60)}$, $\theta_{AB(x=60)} = \theta_{BC(x=60)}$, the equations of the rotation angle and the deflection curve of the beam are obtained.

AB section

$$\theta \approx \frac{1}{EI}\left(-2.1x^4 - 145.7x^3 + 79811x^2 - 3764922x\right) \tag{45}$$

AB section

$$W \approx \frac{1}{EI}\left(-0.4x^5 - 36.4x^4 + 26603.7x^3 - 1882461x^2\right) \tag{46}$$

BC section

$$\theta \approx \frac{1}{EI}\left(-647.5x^3 + 124971.5x^2 - 5571342x + 26980200\right) \tag{47}$$

BC section

$$W \approx \frac{1}{EI}\begin{pmatrix}-161.9x^4 + 41657.2x^3 - 2785671x^2 \\ +26980200x - 303372000\end{pmatrix} \tag{48}$$

By making the rotation angle Eqs. (45) and (47) to be 0 respectively, and selecting the solution that conforms to the

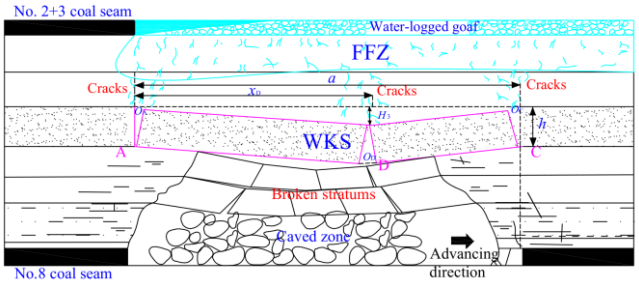

Fig. 10 The shape of surrounding rock after the WKS is broken

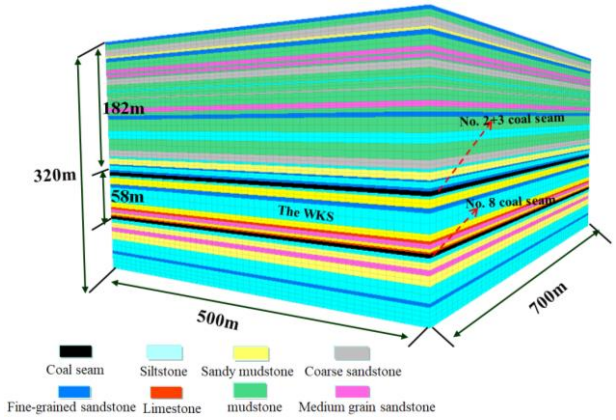

Fig. 11 The Flac3D numerical model

interval, the position of the maximum deflection on the beam is determined: $x_{max} \approx 58.9$ m. In addition, the maximum deflection is obtained: $|W_{max}| \approx 0.0047$ m by using 500 MPa as the elastic modulus E of the WKS (Li. 2011) and then substituting E and x_{max} into Eq. (46). The WKS could yield and break because $|W_{max}| << H_3$, resulting in the possibility of water inrush from the goaf in roof.

After the WKS is broken due to continuous damage, it revolves and sinks, and is overlapped on the stratums that has collapsed below it. Simultaneously, the stratums above it are damaged and the cracks continue to expand, resulting in penetrating the FFZ to form water-conducting channel (Fig. 10). The accumulated water in the goaf needs to pass through the fracture surfaces of the WKS in a large amount to form water inrush. Cognizant to this, after revolving and sinking, the WKS must have sufficiently large crack opening in the broken positions.

There are three fracture surfaces on the broken WKS (Fig. 10), and their opening sizes are O_A, O_C and O_D respectively. Ignoring the breaking angle of the WKS, the following formula can be obtained from the geometric relationship.

$$\begin{cases} O_D = O_A + O_C \\ \dfrac{H_3 - \left(h - \sqrt{h^2 - O_A^2}\right)}{x_D} = \dfrac{O_A}{h} \\ \dfrac{H_3 - \left(h - \sqrt{h^2 - O_C^2}\right)}{a - x_D} = \dfrac{O_C}{h} \end{cases} \tag{49}$$

The opening size is much smaller than the thickness of the WKS in practice. Therefore, formula (49) can be simplified as

$$\begin{cases} O_D = H_3 h \left(\dfrac{1}{a - x_D} + \dfrac{1}{x_D}\right) \\ O_A = \dfrac{H_3 h}{x_D} \\ O_C = \dfrac{H_3 h}{a - x_D} \end{cases} \tag{50}$$

Based on above analysis, substituting $a = 100$ m, $x_D = 64$ m, $h = 21$ m and $H_3 = 1$ m into formula (50), $O_A \approx 0.33$ m, $O_C \approx 0.58$ m and $O_D \approx 0.91$ m. The crack opening that can conduct water is several millimeters generally. In comparison, the crack openings at the three broken positions on the WKS are all larger, increasing the risk of water inrush from the goaf in roof. To sum up, when there is a undrained area of accumulated water in the goaf in Xiqu Mine, the water inrush from the goaf in roof may occur.

4. Numerical analysis of multi-seam mining in Xiqu Mine

The Flac3D numerical software has been generally used to analyze many problems such as rock stratum destruction and roadway deformation in mining engineering compared with discrete element numerical software because its application is more extensive (Azarfar *et al*. 2019, Hu *et al*. 2020, Rinaldi *et al*. 2020, Corkum *et al*. 2020, Darvishi *et al*. 2020, Xue *et al*. 2020, Kong *et al*. 2019). To reproduce the yield process of the WKS and further evaluate water inrush in Xiqu mine, a numerical model of 700 m in length, 500 m in width and 320 m in height was established with the aid of Flac3D. This totaled to 857420 units. In addition, No. 2+3 and No. 8 coal seams were mined successively in numerical model. The grids were densified in the mining affected area to improve the calculation accuracy. The numerical model is shown in Fig. 11. The physical and mechanical parameters of coal seam and rock stratums (Table 2) are estimated from the properties of intact rock by Hoek–Brown failure criterion (Hussian *et al*. 2020, Bahrami *et al*. 2020 Ranjbarnia *et al*. 2020, Carter *et al*. 2020).

To avoid the influence of the boundary, a certain distance was kept between the mined area and the model boundary in the numerical model. Moreover, the Mohr-Coulomb criterion was used to evaluate the failure of rock mass. Based on Fig. 1, the No. 2+3 coal seam was mined first with a coal face length of 130 m. The advancing distance was 50 m for each step. Total advancing distance was 300 m to reach the full mining state. The No. 8 coal seam was then mined with a coal face length of 220 m. The mining distance was 10 m for each step and 300 m in total.

The double-yield model was introduced to fill the goaf in every step of the excavation to simulate the characteristics of the broken rock mass being continuously compacted and the pressure on the floor continuing to

Table 2 The physical and mechanical parameters of coal seam and rock stratums

Stratum	Density /kg·m^{-3}	Bulk modulus /GPa	Shear modulus /GPa	Cohesion /MPa	Internal friction angle /(°)	Tensile strength /MPa
Coal seam	1460	8.86	3.78	1.0	25	4.0
Siltstone	2320	10.1	6.68	1.4	37	6.0
Coarse sandstone	2220	10.1	4.68	1.6	33	7.0
Mudstone	2170	9.80	5.31	1.2	31	5.0
Sandy mudstone	2450	11.0	3.95	1.3	28	5.8
Fine-grained sandstone	2380	12.6	4.88	1.7	35	6.7
Medium grain sandstone	2230	11.5	5.30	1.5	38	7.3
Limestone	2500	13.3	7.60	2.0	32	7.5

(a) 60 m

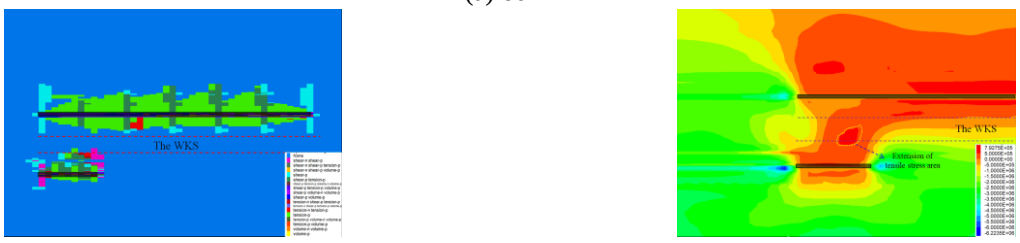

(b) 70 m

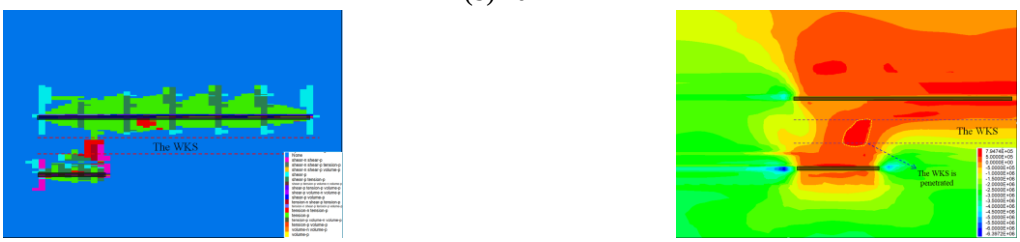

(c) 80 m

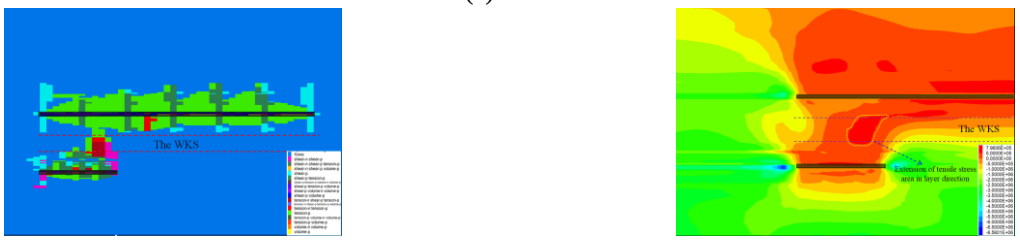

(d) 90 m

Fig. 12 The plastic zone and the minimum principal stress cloud chart when the coal face advances 60 m, 70 m, 80 m and 90 m in No. 8 coal seam

recover in goaf (Wang *et al*. 2018, Kong *et al*. 2019). In the simulation results, a vertical section was made through the midpoint of the coal faces in the two coal seams. The plastic zone and the minimum principal stress cloud chart are shown in Fig. 12.

After mining of No. 2+3 coal seam, the WKS is not affected by the damage from the floor and still maintains continuity. When No. 8 coal seam is mined, the roof stratums are prone to shear failure at the open-off cut and coal face. When the coal face advances 60 m, a tensile

stress area appears at the bottom of the WKS at a point about 40 m away from the open-off cut and the WKS is damaged by tension with a yield height of about 5 m. The tensile stress area and the yield area on the WKS continue to expand forward and upward as mining advances. When advancing is at 70 m, the bottom surface of the WKS is damaged by shearing at the coal face. At 80 m ~ 90 m of advancement, the tensile yield area penetrates the WKS indicating that the WKS has been tensioned and broken. The breaking position is about 60 m ~ 70 m away from the open-off cut. The damage laws of the WKS obtained by numerical analysis and water inrush mechanical model are relatively similar. In both, when the coal face of No. 8 coal seam in the Xiqu Mine advances about 80 m ~ 100 m, the WKS stretch and break at a position 60 m ~ 70 m away from the open-off cut thus increasing the risk of water inrush from goaf in the roof.

5. Analysis of micro-seismic monitoring results

Micro-seismic monitoring is an effective method to analyze the fracture of rock stratums. Through in-depth analysis for the micro-seismic data obtained in the field, the location and form of rock breakage can be identified. The seepage channels in the rock stratums can also be drawn (Ghorbani *et al*. 2018, Zhao *et al*. 2018, Lachaud *et al*. 2019, Officer *et al*. 2020, Zhao *et al*. 2019). In order to evaluate and monitor water inrush, ten micro-seismic sensors were respectively arranged in the transportation lane and return air lane of the first mining panel 18401 in No. 8 coal seam to analyze the breaking laws of the WKS under the multi-seam mining in the Xiqu Mine. The distance between the sensors was about 80 m and thus could accurately locate and capture the micro-fracture events in the surrounding rock during the mining process of No. 8 coal seam. The arrangement of the micro-seismic sensors is shown in Fig. 13.

Between November 3, 2018 and November 30, 2018, the coal face in No. 8 coal seam continued to advance from the open-off cut to the concentrated lane. The micro-seismic monitoring results are shown in Fig. 14. When the coal face advanced 30 m, the rock stratums below the WKS broke in sequence. It was thus determined that micro-fracture events are mainly concentrated below the WKS. Micro-fracture events also occurred at the bottom of the WKS in the open-off cut and the coal face when the coal face advanced to between 50 m and 70 m. At 90 m advancement, many high-magnitude micro-fracture events densely distributed about 70 m away from the open-off cut were detected. This meant that the WKS had broken at this point. The cumulative distribution of micro-fracture events with focal mechanism is shown in Fig. 15 based on in-depth analysis of the focal mechanism. The WKS is prone to shear failure (blue) at the open-off cut and the coal face. It is also prone to tensile failure (red) at a position about 70 m away from the open-off cut (Fig. 15). The analysis results for on-site micro-seismic data are largely consistent with the conclusions obtained by the model calculations. This verifies the reliability of the water inrush mechanical model built. Cognizant to this, when No. 8 coal seam is mined in the Xiqu Mine, it is necessary to actively explore and release the accumulated water in the goaf in No. 2+3 coal seam. It

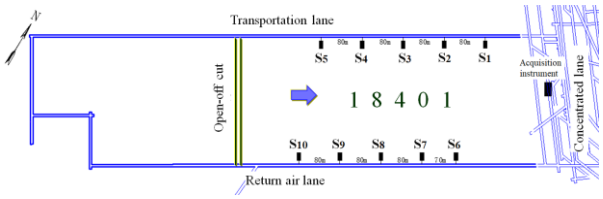

Fig. 13 The arrangement of microseismic sensors in the panel 18401

is also important to ensure that the drainage capacity in the coal face is sufficient to prevent the occurrence of water inrush from goaf in roof.

6. Conclusions

Water-resisting key stratum (WKS) between coal seams is a major barrier that prevents water inrush from goaf in roof during multi-seam mining. A "long beam" water inrush mechanical model was established to analyze the breakage of the WKS in multi-seam mining, in light of the pressure from goaf, the gravity of overburden rock, the gravity of accumulated water, and the constraint conditions based on a case of multi-seam mining of No. 2+3 and No. 8 coal seams in Xiqu Mine. The stress distribution expression of the WKS was derived under different mining distances in No. 8 coal seam (Eqs (11), (12), (26), (27), (28) and (29)). The criterion of breakage at any point of the WKS was obtained by introducing linear Mohr strength theory (Eq. (15)), which could be used to evaluate the water inrush.

• The mechanical model was utilized to assess the fracture of the WKS in Xiqu Mine and its breaking position was calculated. And the risk of water inrush was also evaluated. Moreover, breaking process of the WKS was reproduced using the Flac3D numerical software and was analyzed with on-site microseismic monitoring data. Our results show that when the coal face of No. 8 coal seam in Xiqu Mine advances to about 80 m ~ 100 m, the WKS is stretched and broken at the position of 60 m ~ 70 m away from the open-off cut increasing the risk of water inrush from goaf in roof. This finding matches the result of microseismic analysis confirming the reliability of the water inrush mechanical model built.

• To sum up, when there is a undrained area of accumulated water in the goaf in Xiqu Mine, the water inrush from the goaf in roof may occur. Cognizant to this, when No. 8 coal seam is mined, the accumulated water in the goaf in No. 2+3 coal seam should be released and the drainage in the coal face should be improved to prevent water inrush from goaf in roof. This study therefore provides a theoretical basis for the prevention of water inrush from goaf in roof in Xiqu Mine, and a method for evaluating and monitoring water inrush from goaf in roof.

Acknowledgments

The research described in this paper was financially supported by the National Natural Science Foundation of China (U1710253, 51574059, 52004052 and U1903216).

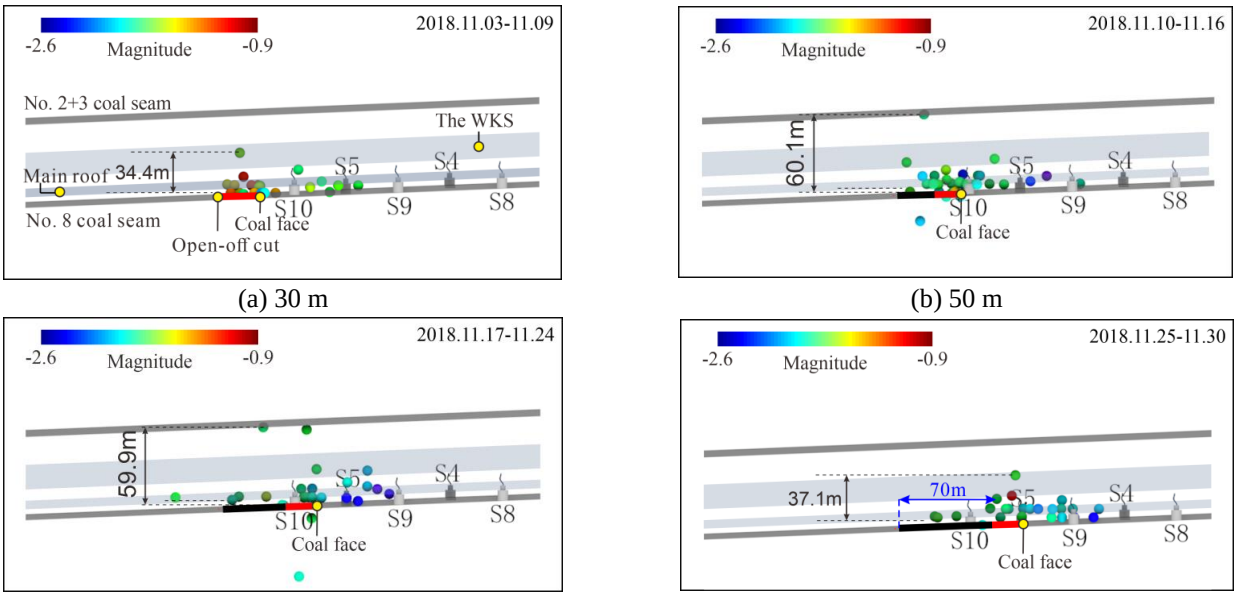

(a) 30 m (b) 50 m

(c) 70 m (d) 90 m

Fig. 14 The distribution of micro-fracture events in the surrounding rock under different advancing distances in No. 8 coal seam

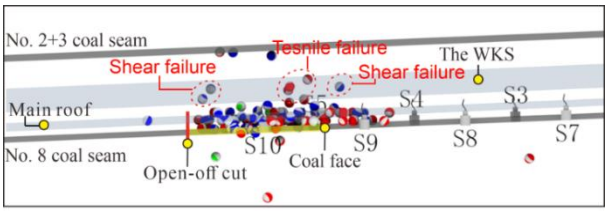

Fig. 15 The cumulative distribution of micro-fracture events with focal mechanism

References

Azarfar, B., Ahmadvand, S., Sattarvand, J. and Abbasi, B. (2019), Stability analysis of rock structure in large slopes and open-pit mine: numerical and experimental fault modeling. *Rock. Mech. Rock. Eng.*, **52**(12), 4889-4905. https://doi.org/ 10.1007/s00603-019-01915-4.

Bahrami, B., Sadatshojaie, A. and Wood, D.A. (2020), "Assessing wellbore stability with a modified lade failure criterion", *J. Energ. Resour-Asme.*, https://doi.org/ 10.1115/1.4046387.

Carter, T.G. and Marinos, V. (2020), "Putting geological focus back into rock engineering design", *Rock. Mech. Rock. Eng.*, https://doi.org/ 10.1007/s00603-020-02177-1.

Chen, B., Zhang, S.C., Li, Y.Y. and Li, J.P. (2020), "Experimental study on water and sand inrush of mining cracks in loose layers with different clay contents", *B. Eng.* Geol. Environ., https://doi.org/ 10.1007/s10064-020-01941-5.

Chen, J.T., Zhao, J.H., Zhang, S.C., Zhang, Y., Yang, F. and Li, M. (2020), "An experimental and analytical research on the evolution of mining cracks in deep floor rock mass", *Pure. Appl. Geophys.*, https://doi.org/10.1007/s00024-020-02550-9.

Chen, L., Zhou, Z.L., Zang, C.W., Zeng, L. and Zhao, Y. (2019), Failure pattern of large-scale goaf collapse and a controlled roof caving method used in gypsum mine. *Geomech. Eng.*, **18**(4), 449-457. https://doi.org/10.12989/gae.2019.18.4.449.

Coal Industry Bureau of China. (2000), *Coal mining regulations and coal pillar design affected by buildings, water bodies, railways and main roadway*. Coal. Industry. Press., Beijing, China.

Corkum, A.G. (2020), "A model for pore pressure response of a claystone due to liberated residual stress dilation", *Rock. Mech. Rock. Eng.*, https://doi.org/ 10.1007/s00603-019-01938-x.

Cui, B.Q., Liu, Y., Feng, G.R., Bai, J.W., Du, X.J., Wang, C.X. and Wang, H.F. (2020), "Experimental study on the effect of fly ash content in cemented paste backfill on its anti-sulfate erosion", *Int. J. Green. Energy*, https://doi.org/ 10.1080/15435075.2020.1791877.

Darvishi, A., Ataei, M. and Rafiee, R. (2020), "Investigating the effect of simultaneous extraction of two longwall panels on a maingate gateroad stability using numerical modeling", *Int. J. Rock. Mech. Min.*, https://doi.org/ 10.1016/j.ijrmms.2019.104172.

Dou, L.M., He, J., Gong, S.Y., Song, Y.F. and Liu, H. (2012), A case study of micro-seismic monitoring: goaf water-inrush dynamic hazards. *J. China. Univ. Mining. Technol.*, **41**(1), 20-25.

Feng, G.R., Bai, J.W., Yang, W.B., Wang, S.Y. and Kang, L.X. (2019), "Influence of multiple mining damage on the stability of water-resisting control strata", *J. China. Coal. Soc.*, **44**(3), 777-785. https://doi.org/ 10.13225/j.cnki.jccs.2018.6042.

Gee, D., Bateson, L., Grebby, S., Novellino, A., Sowter, A., Wyatt, L., Marsh, S., Morgenstern, R. and Athab, A. (2020), "Modelling groundwater rebound in recently abandoned coalfields using DInSAR", *Remote. Sens. Environ.*, https://doi.org/ 10.1016/j.rse.2020.112021.

Ghorbani, S., Barari, M. and Hoseini, M. (2018), "Presenting a new method to improve the detection of micro-seismic events", *Environ. Monit. Assess.*, https://doi.org/ 10.1007/s10661-018-6837-6.

Huang, W.P., Li, C., Zhang, L.W., Yuan, Q., Zheng, Y.S. and Liu, Y. (2018), "In situ identification of water-permeable fractured zone in overlying composite strata", *Int. J. Rock. Mech. Min. Sci.*, **105**, 85-97. https://doi.org/ 10.1016/j.ijrmms.2018.03.013.

Hu, B., Sharifzadeh, M., Feng, X.T., Talebi, R. and Lou, J.F. (2020), "Ground support performance in deep underground mine with large anisotropic deformation using calibrated numerical simulation (case of mine-H)", *Geomech. Eng.*, **21**(6), 551-564. https://doi.org/ 10.12989/gae.2020.21.6.551.

Hussian, S., Mohammad, N., Rehman, Z.U., Khan, N.M.

Shahzada, K. Ali, S. Tahir, M. Raza, S. and Sherin, S. (2020), "Review of the geological strength index (GSI) as an empirical classification and rock mass property estimation tool: origination, modifications, applications, and limitations", *Adv. Civ. Eng*., https://doi.org/ 10.1155/2020/6471837.

Jiang, J.Q., Zhang, P.P., Nie, L.S., Li, H., Xu, L.N. and Wang, W.D. (2014), "Fracturing and dynamic response of high and thick stratas of hard rocks", *Chin. J. Rock. Mech. Eng*., **33**(7), 1366-1374. https://doi.org/ 10.13722/j.cnki.jrme.2014.07.008.

Jiang, J.Q., Zhang, P.P., Qin, G.P. and Xu, B. (2015), "Analysis of destabilized fracture and microseismic activity of high-located main key strata", *Rock. Soil. Mech.*, **36**(12), 3567-3575. https://doi.org/ 10.16285/j.rsm.2015.12.029.

Kong, P., Jiang, L.S., Shu, J.M., Sainoki, A. and Wang, Q.B. (2019), "Effect of Fracture heterogeneity on rock mass stability in a highly heterogeneous underground roadway", *Rock. Mech. Rock. Eng*., **52**(11), 4547–4564. https://doi.org/ 10.1007/s00603-019-01887-5.

Kromkova, M. and Seko, M. (2020), "Drainage of the 12th mining field in the Handlova Mine (Slovakia)", *Mine. Water. Environ.*, **39**(2), 416-422. https://doi.org/ 10.1007/s10230-020-00672-z.

Lachaud, C., Marsan, D., Montagnat, M., Weiss, J., Moreau, L. and Gimbert, F. (2019), "Micro-seismic monitoring of a shear fault within a floating ice plate", *J. Geophys. Res-Sol. Ea.*, **124**(10), 10444-10467. https://doi.org/ 10.1029/2019JB018339.

Li, B. (1999), "'Down three zone' for predicting water invasion from coal bed floor aquifer theory, development and application", *J. Shandong. Univ. Sci. Technol. (Nat Sci)*., **18**(4), 11-18. https://doi.org/ 10.16452/j.cnki.sdkjzk.1999.04.004.

Li, J.P. (2011), *Mining rock mechanics*. Metallurgical. Industry. Press., Beijing, China.

Liu, S.L., Li, W.P. and Wang, Q.Q. (2018), "Height of the water-flowing fractured zone of the jurassic coal seam in northwestern China", *Mine. Water. Environ*., **37**(2), 312-321. https://doi.org/ 10.1007/s10230-017-0501-1.

Li, Z.L., Shan, R.L. Wang, C.H. Yuan, H.H. and Wei, Y.H. (2020), "Study on the distribution law of stress deviator below the floor of a goaf", *Geomech. Eng*., **21**(3), 301-313. https://doi.org/ 10.12989/gae.2020.21.3.301.

Li, Z., Xu, J.L., Ju, J.F., Zhu, W.B. and Xu, J.M. (2018), "The effects of the rotational speed of voussoir beam structures formed by key strata on the ground pressure of stopes", *Int. J. Rock. Mech. Min. Sci*., **108**, 67-79. https://doi.org/ 10.1016/j.ijrmms.2018.04.041.

Ma, Q., Tan, Y.L., Liu, X.S., Gu, Q.H. and Li, X.B. (2020), "Effect of coal thicknesses on energy evolution characteristics of roof rock-coal-floor rock sandwich composite structure and its damage constitutive model", *Compos. Part. B-Eng*., https://doi.org/10.1016/j.compositesb.2020.108086.

Officer, T. and Secco, R.A. (2020), "Detection of high P,T transformational faulting in Fe2SiO4 via in-situ acoustic emission: relevance to deep-focus earthquakes", *Phys. Earth. Planet. In,* https://doi.org/ 10.1016/j.pepi.2020.106429.

Qian, M.G. (2010), *Mine pressure and rock formation control*. China. University. of. Mining. and. Technology. Press., Xuzhou, China.

Qu, Q.D., Xu, J.L., Wu, R.L., Qin, W. and Hu, G.Z. (2015), "Three-zone characterization of coupled strata and gas behavior in multi-seam mining", *Int. J. Rock. Mech. Min. Sci*., **78**, 91-98. https://doi.org/ 10.1016/j.ijrmms.2015.04.018.

Ranjbarnia, M., Rahimpour, N. and Oreste, P. (2020), "A new analytical-numerical solution to analyze a circular tunnel using 3D Hoek-Brown failure criterion", *Geomech. Eng.*, **22**(1), 11-23. https://doi.org/ 10.12989/gae.2020.22.1.011.

Rashid, M.I., Benhelal, E. and Rafiq, S. (2020), "Reduction of greenhouse gas emissions from gas, oil, and coal power plants in Pakistan by carbon capture and storage (CCS): a review", *Chem. Eng. Technol*., https://doi.org/ 10.1002/ceat.201900297.

Ray, S.K. and Singh, R.P. (2007), "Recent developments and practices to control fire in undergound coal mine", *Fire. Technol*., **43**(4), 285-300. https://doi.org/ 10.1007/s10694-007-0024-6.

Rinaldi, A.P. and Urpi, L. (2020), "Fault reactivation induced by tunneling activity in clay material: Hints from numerical modeling", *Tunn. Undergr. Sp. Tech*., https://doi.org/ 10.1016/j.tust.2020.103453.

Song, W.C., Liang, Z.Z., Liu, W.T. and Zhao, C.B. (2019), "Theoretical analysis and experimental investigation on failure characteristics and stability of stope floors", *Chin. J. Rock. Mech. Eng*., **38**(11), 2208–2218. https://doi.org/ 10.13722/j.cnki.jrme.2019.0259.

Srivastava, S., Pal, S.K. and Kumar, R. (2020), "A time-lapse study using self-potential and electrical resistivity tomography methods for mapping of old mine working across railway-tracks in a part of Raniganj coalfield, India", *Environ. Earth. Sci*., https://doi.org/ 10.1007/s12665-020-09067-3.

Szurgacz, D., Tutak, M., Brodny, J., Sobik, L. and Zhironkina, O. (2020), "The method of combating coal spontaneous combustion hazard in goafs-a case study", *Energies*., https://doi.org/ 10.3390/en13174538.

Wang, C.X., Jiang, N., Shen, B.T., Sun, X.Z., Zhang, B.C., Lu, Y. and Li, Y.Y. (2019), "Distribution and evolution of residual voids in longwall old goaf", *Geomech. Eng*., **19**(2), 105-114. https://doi.org/ 10.12989/gae.2019.19.2.105.

Wang, F., Xu, J.L., Chen, S.J. and Ren, M.Z. (2019), "Method to predict the height of the water conducting fractured zone based on bearing structures in the overlying strata", *Mine. Water. Environ*., **38**(4), 767-779. https://doi.org/ 10.1007/s10230-019-00638-w.

Wang, P., Jiang, F.X., Feng, Z.Q. and Wang, D.Z. (2011), "Relationship between fracture of high-position thick and hard roof and mine quake forecast", *Chin. J. Geotech. Eng*., **33**(4), 618-623.

Wang, P., Zhao, J., Feng, G. and Wang, Z. (2018), "Interaction between vertical stress distribution within the goaf and surrounding rock mass in longwall panel systems", *J. S. Afr. I. Min. Metall*., **118**(7), 745-756. https://doi.org/ 10.17159/2411-9717/2018/v118n7a8.

Wu, Q. (2014), "Progress, problems and prospects of prevention and control technology of mine water and reutilization", *J. China Coal. Soc*., **39**(5), 795-805. https://doi.org/ 10.13225/j.cnki.jccs.2014.0478.

Wu, Q., Xu, H., Zhao, Y.W. and Cui, J.Q. (2016), "Dynamic visualization and prediction for water bursting on coal roof based on "three maps method", *J. China Coal. Soc*., **41**(12), 2968-2974. https://doi.org/ 10.13225/j.cnki.jccs.2016.0392.

Xue, Y.C., Sun, W.B. and Wu, Q.S. (2020), "The influence of magmatic rock thickness on fracture and instability law of mining surrounding rock", *Geomech. Eng*., **20**(6), 547-556. https://doi.org/ 10.12989/gae.2020.20.6.547.

Xue, Y.C., Wu, Q.S. and Sun D.Q. (2020), "Numerical investigation on overburden migration behaviors in stope under thick magmatic rocks", *Geomech. Eng*., **22**(4), 349-359. https://doi.org/ 10.12989/gae.2020.22.4.349.

Xu, J.L., Zhu, W.B. and Wang, X.Z. (2012), "New method to predict the height of fractured water-conducting zone by location of key strata", *J. China Coal. Soc*., **37**(5), 762-769. https://doi.org/ 10.13225/j.cnki.jccs.2012.05.002.

Yin, L.M., Ma, K., Chen, J.T., Xue, Y.C., Wang, Z.Q. and Cui, B.Q. (2019), "Mechanical model on water inrush assessment related to deep mining above multiple aquifers", *Mine. Water. Environ*., **38**(4), 827-836. https://doi.org/ 10.1007/s10230-019-00623-3.

Zhang, S.C., Shen, B.T., Zhang, X.G., Li, Y.Y., Sun, W.B. and

Zhao, J.H. (2020), "Modelling the coupled fracture propagation and fluid flow in jointed rock mass using FRACOD", *Geomech. Eng*., **22**(6), 529-540. https://doi.org/ 10.12989/gae.2020.22.6.529.

Zhao, Y., Yang, T.H., Bohnhoff, M., Zhang, P.H., Yu, Q.L., Zhou, J.R. and Liu, F.Y. (2018), "Study of the rock mass failure process and mechanisms during the transformation from open-pit to underground mining based on microseismic monitoring", *Rock. Mech. Rock. Eng*., **51**(5), 1473-1493. https://doi.org/ 10.1007/s00603-018-1413-5.

Zhao, Y., Yang, T.H., Zhang, P.H., Xu, H.Y. and Wang, S.H. (2019), "Inversion of seepage channels based on mining-induced microseismic data", *Int. J. Rock. Mech. Min. Sci*., https://doi. 10.1016/j.ijrmms.2019.104180.

CC